Special Feature: Metallic Materials

Research Report

Prediction of Transformation Kinetics of Ferrite-Pearlite-Bainite in Medium Carbon Forging Steel

Hideaki Ikehata, Kouji Tanaka and Carlos Capdevila

Report received on Aug. 3, 2012

ABSTRACT Successive transformations were modeled to predict the mixed microstructure of ferrite (α), pearlite (*P*) and bainite (*B*) in medium-carbon forging steels. The kinetics of diffusional transformations were calculated based on the classical nucleation and growth theory coupled with CALPHAD multicomponent thermodynamics. The parabolic growth rate of proeutectoid α includes a time dependence due to carbon enrichment in the interior of austenite (γ) grains, and the γ/α interface was assumed to be under constrained local equilibrium with respect to the alloyed manganese. The kinetics of *P* nucleation on the γ/α surface was integrated into the model. The thermodynamic calculation determined the chemical free energies of untransformed γ during the preceding transformations. The inclusion of bainite was predicted based on energy criteria for the nucleation and diffusionless growth of bainitic α. The developed model was validated experimentally for commercial manganese steel (ASTM1538). A log-normal distribution of γ grain size (d_0) was employed to account for local variations in C enrichment, and was found to well reproduce the onset of the *P* and *B* transformations. With increasing Mn content, average d_0 and cooling rate, the fraction of *B* increases. The agreement was satisfactory and the model provided practical hot forging conditions for avoiding the formation of *B* in final products.

KEYWORDS Phase Transformations, Kinetics Modeling, Medium-carbon Forging Steel, Continuous-cooling, Multicomponent Thermodynamics, Proeutectoid Ferrite, Pearlite, Bainite

1. Introduction

Medium-carbon steels are used in large quantities as raw materials for various hot-forged auto parts. The chemical composition of the steel and its cooling rate after forging determines its non heat-treated microstructure, consisting of proeutectoid ferrite (α) and pearlite (*P*). The *P* forms below the eutectoid temperature following the austenite (γ) to α transformation. The final α and *P* fractions have a primary effect on the average hardness, which is an index of the balanced proof strength and machinability of the forged product. Below the eutectoid temperature, a mixture of bainitic ferrite (α_B) and fine cementite precipitates is also a form of transformation product called bainite (*B*). It is relatively hard and its inclusion in the α + *P* microstructure degrades the machinability.

From the standpoint of global production, it is of some concern that the composition variability of steel supplies is becoming larger. In many commercial grades of medium-carbon forging steel (MCFS), alloying elements such as Mn must also be controlled. In addition, faster cooling of forged workpieces will be required due to space-saving factory designs. Such increased cooling rates may give rise to *B* formation even in forgings with slight Mn variations, which has not been a problem to date. Therefore, computational predictions of successive α-*P*-*B* transformations are required in order to promptly deal with modified steel supplies and forging conditions.

The "subunit model" has been proposed by Bhadeshia and coworkers[1-6] to describe the isothermal kinetics of the *B* transformation at austenite (γ) grain boundaries. It involves self-catalytic nucleation and diffusionless growth to a fixed volume of α_B subunit plates momentarily. Although whether the mechanism is diffusional or diffusionless remains controversial for *B*, α_B subunit formation can be interpreted as a combination of the driving force for nucleation and a free energy change in a γ phase with the same chemical composition. These two energy criteria for the onset of

the *B* transformation have been simply formulated from observations of the *B*-start temperature for various steels.[1,7]

In view of the composition range of MCFS, it is reasonable to assume that under practical cooling rates, the remainder of the γ occupied by α and *P* produces upper bainite. Therefore, the onset of the *B* transformation following the α-*P* transformation is expected when the energy criteria are met for the untransformed austenite (γ_U). However, the chemistry of γ_U depends on preceding transformations and no evidence has been reported as to the validity for the existence of *B* within the α + *P* microstructure.

This paper aims to build a model that can accurately calculate the evolution of the α + *P* fraction during continuous cooling of MCFS, and to attempt to predict the fraction of *B* by applying the above energy criteria to γ_U.

2. Model and Calculation Methods

2. 1 Framework of the Model

Much effort has been devoted to understanding the kinetics of phase transformations in steels. There are a number of integrated models[8-11] that can reportedly predict the evolution of α, *P*, widmanstätten ferrite, and *B*. These models are based on classical nucleation and growth theories (CNGT) developed originally for the Fe-C binary system. With regard to the production of low-carbon sheet steels, such models focus on controlling the grain size of α, which significantly affects the mechanical strength and elongation.

The present model for MCFS also uses the equations proposed in CNGT. In particular, to accurately predict the α and *P* fractions, the effects of the Mn content have been studied extensively with respect to the partitioning between γ and α. Since the α nucleates mostly on the surface of γ grain boundaries, the grain size (d_0) is an important input, in addition to the chemical composition and cooling rate. Immediately following hot forging, new γ grains are recrystallized and grain growth begins. From the hot working parameters, d_0 can be estimated using the empirical equations.[12]

In the following sections, the kinetic equations are derived for isothermal phase transformations. An extension to continuous cooling is made by assuming the additivity rule. More specifically, the volume increments of the transformed α and *P* are calculated and integrated for small isothermal time steps in a segmented cooling schedule. In this scheme, thermodynamic conditions discussed in the next section are evaluated with changing temperatures in each time step.

2. 2 Multicomponent Thermodynamic Calculation

The thermodynamic effects of alloying elements are of great importance in the kinetics of diffusional transformation. Due to thermodynamic interactions in a multicomponent system, the addition of Mn and/or Si affects the activity of C, which determines the stability of γ and the γ/α phase equilibrium. The CALPHAD method was developed on the basis of modeling the chemical free energy, and has now become the standard tool for the calculation of multicomponent thermodynamics. One of the commercial packages, *Thermo-Calc* (*TC*), was employed in the present work with the aid of the programming interface, *TQ-i*. Coupled with the thermodynamic database *TCFe3* and the mobility database *MOB2*, the maximum driving force (ΔG_{max}) for α precipitation, the equilibrium γ/α composition sets, and C diffusivities in γ (D_C^{γ}) were calculated for a given composition of the Fe-C-Si-Mn-Cr system.

In the CNGT, the nucleation and growth of α and/or cementite (θ) in *P* are basically treated as C diffusion-controlled processes. For the alloy system considered, however, two extremes of constrained equilibrium were considered for determining the local interface C concentrations ($X_C^{\gamma/\alpha}$, $X_C^{\alpha/\gamma}$, $X_C^{\gamma/\theta}$). In particular, Mn is a substitutional solution element and has a diffusivity in γ thousands of times smaller than that of C. If no partitioning of Mn occurs, para-equilibrium (PE) is established, in which only the chemical potentials of C are equated between the γ and product α phases. In contrast, spike-like Mn partitioning only on the γ side of the interface leads to negligible partitioned local equilibrium (NPLE). In both cases, the Mn concentration in the α (θ) is identical to that in the γ.

The constrained equilibria were calculated with *TC* by setting *zero* moles of α (θ) to give a hypothetical average composition on the γ/(γ + α) or γ/(γ + θ) boundary and by equating the chemical potentials of C and Mn concentration in γ and α (θ). **Figure 1** shows an example of the calculated C concentration at the γ/α interface under PE and NPLE conditions. The alloy compositions are Fe-0.39%C-1.3%Mn, Fe-0.39%C-1.5%Mn and Fe-0.39%C-1.7%Mn, and $X_C^{\gamma/\alpha}$ and $X_C^{\alpha/\gamma}$

are interpolated on the vertical section of the Fe-C-Mn phase diagram. It can be clearly seen that minor variations in the Mn content leads to larger differences in $X_C^{\gamma/\alpha}$ for NPLE than for PE.

2. 3 Kinetics of Proeutectoid Ferrite

The incubation time (τ) for the isothermal α transformation was calculated using Eq. 1 according to the pillbox nucleus theory.[13] The γ/α interfacial energy ($\sigma^{\gamma/\alpha}$) and the volume occupied by an iron atom (v^{α}) in α were assumed to be 0.705 J/m^2 and 8.785 × 10^{-30} m^3, respectively.[14] The average lattice parameter (a) for γ and α was estimated from the experimental polynomials[15] including the effect of alloying elements. The driving force per unit volume (ΔG_V) for α precipitation is equal to ΔG_{max} divided by the molar volume (V_m). X_C^0 is the initial C content and other symbols have their usual meaning.

$$\tau = \frac{12kTa^4 \cdot \sigma^{\gamma/\alpha}}{D_C^{\gamma} X_C^0 \cdot v_{\alpha}^2 \cdot \Delta G_V^{\ 2}} \quad \cdots\cdots\cdots\cdots\cdots\cdots (1)$$

The nucleation rate (I) of α at γ grain boundaries was calculated using Eq. 2.[8] The parameter K_1 (1.739 × 10^{26} K$^{0.5}$/m^4) is related to the density of nucleation sites, and K_2 (6.6 × 10^8 J^3/mol^3) is a geometric factor for α nuclei and includes the ratio of the interfacial energies for coexisting γ/α and γ/γ [16] interfaces. In view of the typical α network microstructure of MCFS, the nucleation of α was assumed to take place only on γ grain surfaces. Therefore, site saturation was realized when the growing α grains covered the entire surface area during the calculation.

$$I = \frac{K_1(1-X_C^{\gamma})D_C^{\gamma}}{\sqrt{T}} \exp\left(-\frac{K_2}{RT\Delta G_V^2}\right) \cdots\cdots\cdots (2)$$

The C swept by the motion of the γ/α interface diffuses into the γ grain. Assuming that C diffusion controls the growth of α, the one-dimensional growth rate is theoretically parabolic and the rate constant (α_1) can be expressed by Eq. 3, which can be solved numerically.[17] Conventionally, the C concentrations at the γ/α interface ($X_C^{\gamma/\alpha}$, $X_C^{\alpha/\gamma}$) has been calculated under the fixed PE constraint for low C steels. However, the issue has received renewed attention during the last decade, and the alternate condition of PE or NPLE, depending on the transformation temperature, has been proposed for Fe-C-Mn and Fe-C-Ni alloys.[18-21]

$$2\sqrt{\frac{D_C^{\gamma}}{\pi}} \frac{X_C^{\gamma/\alpha} - X_C^{\gamma}}{X_C^{\gamma/\alpha} - X_C^{\alpha/\gamma}} = \alpha_1 \exp\left\{\frac{\alpha_1^{\ 2}}{4D_C^{\gamma}}\right\} erf\left\{\frac{\alpha_1}{2\sqrt{D_C^{\gamma}}}\right\} \cdots\cdots\cdots\cdots (3)$$

For 0.37%C-1.45%Mn steel, the authors reported that the calculated PE kinetics provided an α-fraction evolution far faster than that experimentally observed during isothermal annealing at 973 K.[24] A local equilibrium transition from PE to NPLE was one

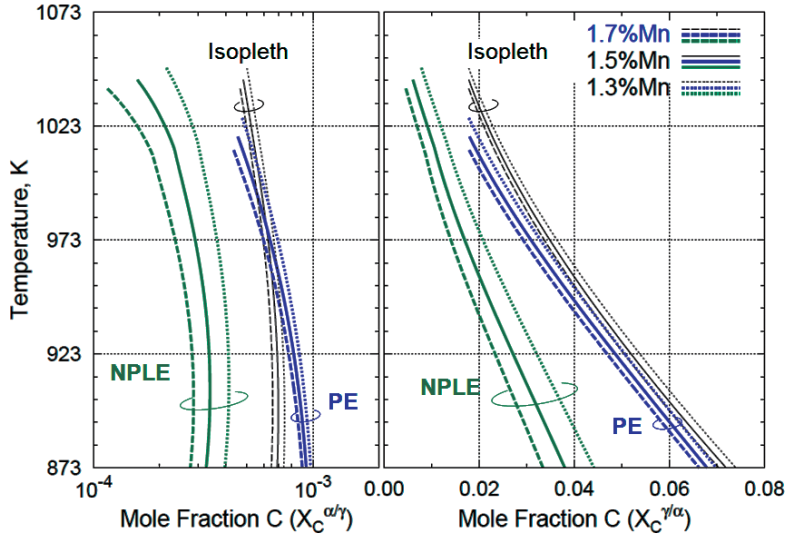

Fig. 1 Calculated effect of Mn content on γ/α para-equilibrium (PE) and negligible partitioning local equilibrium (NPLE).

possible means of interpreting the experimental kinetics. In this process, a spike in the Mn concentration occurs in the γ adjacent to the interface; this is possible when the interface migrates slowly enough. A detailed analysis concluded that the time when PE prevailed was short and most of the growth kinetics were governed by NPLE.

In fact, a small change in the Mn content of MCFS significantly affects the α fraction in real forgings. As shown in Fig. 1, such an effect can be explained most reasonably under NPLE in terms of the large shift of $X_C^{\gamma/\alpha}$. Therefore, in this work, NPLE conditions were adopted throughout the α transformation process during continuous cooling.

"Soft impingement" occurs in the interior of a γ grain when the C diffusion originating from the growing α on the other side of the grain boundary, and the C enrichment of γ_U gradually decreases the growth rate. The regressive mean-field approximation was implemented to take such a soft impingement effect into account. The increase in C content away from the interface (X_C^{γ}) was approximated by updating the average C content in γ (X_{Cbar}^{γ}). By using Eq. 4, an increase in the volume fraction of α (V_f) makes α_1 time-dependent. In the same sense, other parameters for I were also recalculated by inputting a new X_{Cbar}^{γ}.

$$X_C^{\gamma} \approx X_{Cbar}^{\gamma} = \frac{X_C^0 - V_f X_C^{\alpha/\gamma}}{1 - V_f} \quad \cdots\cdots\cdots\cdots (4)$$

V_f was calculated in the following manner.[8] The cooling schedule was segmented into small time steps (Δt) during which the temperature was T_i ($i = 1, \ldots k, \ldots n$). The α grains nucleating on γ grain surfaces grow as half ellipsoids, collide with each other, and finally acquire a film-like morphology. The short radius (R) of an α grain, nucleated at a temperature T_k and grown until T_n, is given by:

$$R^2(T_n, T_k) = \sum_{i=k}^{n} \left\{ \alpha_1{}^2(T_i) \cdot \Delta t \right\}. \quad \cdots\cdots\cdots\cdots (5)$$

Due to the preferential growth on γ grain surfaces, the long radius is three-times longer than R in average. At a normal distance y from the grain surface, the sum of the cross-sectional areas of the α ellipsoids (Y^{ex}) is expressed by Eq. 6.

$$\begin{aligned} Y^{ex} &= 0 \quad \text{for } y > R(T_n, T_k) \\ &= \sum_{i=1}^{k} I \cdot \Delta t \cdot \pi \sum_{i=k}^{n} \left\{ 9R^2(T_n, T_k) - y^2 \right\} \quad \text{for } y < R(T_n, T_k) \end{aligned} \quad \cdots\cdots\cdots\cdots (6)$$

Using the extended area/volume concept, V_f at T_n is calculated as the integral of y from 0 to the maximum R.

$$V_f(T_n) / V_f^{eq}(T_n) = 1 - \exp\left[-2S_V \int_0^{R(t_n, t_1)} \left\{ 1 - \exp\left(-Y^{ex} \right) \right\} dy \right] \quad \cdots\cdots\cdots\cdots (7)$$

The result is then multiplied by the γ grain-boundary area per unit volume (S_V), which is estimated to be $2.37/d_0$ for truncated octahedral γ grains. The calculated V_f needs to be normalized with respect to the equilibrium fraction V_f^{eq} defined by the lever rule.

2. 4 Kinetics of Pearlite

Before the P transformation occurs, the film-like α covers most of the γ grain-boundary area. Therefore, the kinetics of P were modeled following the comprehensive work by Capdevila et al.[22] on P nodules formed at the γ/α interface. The thermodynamic condition for the onset of the P transformation is that X_{Cbar}^{γ} be higher than the γ/(γ + θ) equilibrium concentration:

$$X_C^{\gamma/\theta} \le X_{Cbar}^{\gamma}. \quad \cdots\cdots\cdots\cdots (8)$$

In addition, the formation of P nodules is possible if the velocity of the migrating γ/α interface ($v^{\alpha/\gamma}$) is slow enough to allow the nucleation of cementite (θ) particles. The critical velocity has been analyzed by Aaronson et al.[23]

$$v^{\alpha/\gamma} = \alpha_1 / 2\sqrt{t} \le \frac{-\left(a^{\gamma}\right)^3 D_C^{\gamma} X_C^{\gamma/\theta} \left(\Delta G_V^{\theta}\right)^3}{16\left(1 - \sigma^{\alpha/\theta}/2\sigma^{\alpha/\gamma}\right)\sqrt{\pi kT\left(\sigma^{\alpha/\theta}\right)^5 K}} \quad \cdots\cdots\cdots\cdots (9)$$

$$\Delta G_V^{\theta} = 6.914 \cdot 10^8 \cdot \left(A_e 1 - T \right) / A_e 1, \ \text{J/m}^3 \quad \cdots\cdots\cdots\cdots (10)$$

In Eq. 9, a^{γ} is the lattice parameter in γ and $\Delta G^{\theta}{}_V$ is the

volume free energy change associated with θ nucleation. The latter is conveniently given by Eq. 10. K is a constant (1.0×10^{-4}) and $\sigma^{\alpha/\theta}$ is the interfacial energy (0.68 J/m^2) of the α/θ interface.

The nucleation rate of P (I_P) was formulated in a similar manner [24] to that of α nucleation from γ grain surfaces, edges, and corners. The growth of P in Fe-Mn-C alloys has been discussed in several papers.[22,25,26] It was proposed that, depending on the temperature, the operating mechanism changes from one involving full partitioning of Mn between γ/α and γ/θ (Mn-diffusion controlled) to NPLE (C-diffusion controlled). Since Mn partitioning is unlikely for practical cooling rates during forging, the NPLE expression was adopted for the P growth rate (G).

The C concentration at the γ/θ interface in Eq. 11 was given by TC under the NPLE constraint, as described for the γ/α interface. The expressions for the P lamellar spacings (S, S_c) were taken from the literature.[27]

$$G = \frac{D_C^{\gamma}}{0.72}\frac{S}{S_\alpha S_\theta}\frac{X_C{}^{\gamma/\alpha} - X_C{}^{\gamma/\theta}}{X_C{}^{\theta/\gamma} - X_C{}^{\alpha/\gamma}}\left(1-\frac{S_c}{S_0}\right) \cdots\cdots (11)$$

In Eq. 12, the volume fraction of P (V_P) was integrated assuming a hemispherical geometry for the nodules. The α/γ interface area ($S^{\alpha/\gamma}$) depends on V_f at this point and was estimated using the expression: $S_V(1 - V_f)^{2/3}$. The parameter ϕ is an integral constant that equals y/G, where y is the normal distance from the surface of the α grain. V_P^{eq} is the equilibrium fraction of P defined in the relation:

$$f(G, I_P, T_n) = \int_0^1 \left[1 - exp\left\{\frac{\pi}{3} I_P \sum_{i=k}^{n} G^2(T_i)\Delta t^3\left(1 - 3\phi^2 - 2\phi^3\right)\right\}\right] d\phi$$

$$V_P(T_n)/V_P^{eq} = 1 - exp\left\{S_V^{\alpha/\gamma}\sum_{i=k}^{n} G(T_i)\Delta t \cdot f(G, I_P, T_n)\right\}. \cdots\cdots (12)$$

From this expression, V_P^{eq} equals $1.0 - V_f^{eq}$ at the onset of the P transformation and becomes unity at lower temperature where $X_C^{\gamma/\theta}$ becomes equal to the bulk C content (X_C^0).

$$V_P^{eq} = \frac{X_C{}^0 - X_C{}^{\alpha/\gamma}(T_n)}{X_C{}^{\gamma/\theta}(T_n) - X_C{}^{\alpha/\gamma}(T_n)} \cdots\cdots (13)$$

2. 5 Start Condition of Bainite

The two energy criteria for the onset of the B transformation are: i) the driving force for α nucleation (ΔG_{max}) becomes larger than the universal nucleation function (GN), irrespective of the steel composition, and ii) the free energy change associated with diffusionless growth ($\Delta G^{\gamma\rightarrow\alpha B}$) exceeds the stored energy of the B.

These criteria were first applied to the remaining γ_U. In the course of the α transformation, X_{Cbar}^{γ} increases in accordance with Eq. 4. A high X_{Cbar}^{γ} stabilizes the γ_U and ΔG_{max} becomes small. This hinders the formation of α_B during continuous cooling and causes the B transformation to occur at lower temperatures. The G_N reviewed for high-carbon steels[7] was found to be appropriate for predicting the B transformation in C-enriched γ_U.

$$GN(T) = 3.5463 \cdot T - 3499.4 \text{ J/mol} \cdots\cdots (14)$$

On the other hand, $\Delta G^{\gamma\rightarrow\alpha B}$ was calculated simply from the difference in free energies between γ_U and α with the same chemical composition. An incremental evaluation of X_{Cbar}^{γ} enables the accurate calculation of $\Delta G^{\gamma\rightarrow\alpha B}$ available for the onset of the B transformation.

3. Experimental Procedures

3. 1 Materials and Austenitization

Cylindrical specimens 8 mm in diameter and 12 mm in height were machined from three types of ASTM1538 steel bars. Their chemical compositions are listed in **Table 1**, and they are labeled HM, S, and LM. Compared to the standard S steel, the Mn content of the HM and LM steels deviates by about 0.2 mass%.

The transformation kinetics of the steels were analyzed using a hydraulic hot-working simulator. The temperature was measured using a 0.2-mm-diameter thermocouple welded onto the specimen. After austenitizing at various temperatures, the specimens

Table 1 Chemical composition of three ASTM1538 steels.

	C	Si	Mn	Ni	Mo	Cr	Cu	Al
HM	0.39	0.51	1.69	0.07	-	0.15	0.12	0.009
S	0.39	0.50	1.51	0.05	0.01	0.14	0.03	0.009
LM	0.39	0.51	1.29	0.06	-	0.15	0.11	0.008

were compressed at 1373 K to 50% of their original height, and a few seconds later were rapidly cooled to 1033 K, slightly above the Ae3 temperature. Some of the specimens were then quenched using a He-gas jet in order to examine the γ grain size (d_0) just before the transformation.

3. 2 Measurement of Austenite Grain Size Distribution

In the present kinetics model, the local variations in d_0 in real polycrystalline samples were taken into account. If all of the γ grain boundaries are decorated by the proeutectoid α, a finite volume of γ_U is isolated. Subsequently, the smaller d_0 is, the faster X_{Cbar}^{γ} increases. X_{Cbar}^{γ} is one of the decisive factors for the onset of the *P* transformation and the driving force for α_B nucleation. Therefore, the successive transformations can be better described by calculating the thermodynamics for discrete groups of d_0 values in accordance with its distribution.

Micrographs of the He-quenched samples were obtained using standard metallographic techniques, and the d_0 distribution was measured using image analysis software. As seen in **Fig. 2**, a statistical analysis showed that a log normal distribution (LND) curve fit well to the measurements. In the calculation, the number frequency of the *i*-th d_0 ($f(d_{0,i})$) is generated using the well-known LND relation based on the statistical average and standard deviation. Then the volume contribution of *i*-th group of $d_{0,i}$ was calculated using:

$$dV(d_{0,i}) = d_0^3 \cdot f(d_0) \Big/ \sum_i \left\{ d_{0,i}^3 \cdot f(d_{0,i}) \right\} \quad \cdots\cdots (16)$$

Although from Fig. 2, the average d_0 is 57 μm, it should be emphasized that larger γ grains having a d_0 of more than 100 μm occupy a major fraction of the total volume. In the following, the kinetics calculations were carried out for each d_0 group until the total transformed volume fraction (α + *P* + *B*) matched the corresponding $dV(d_{0,i})$.

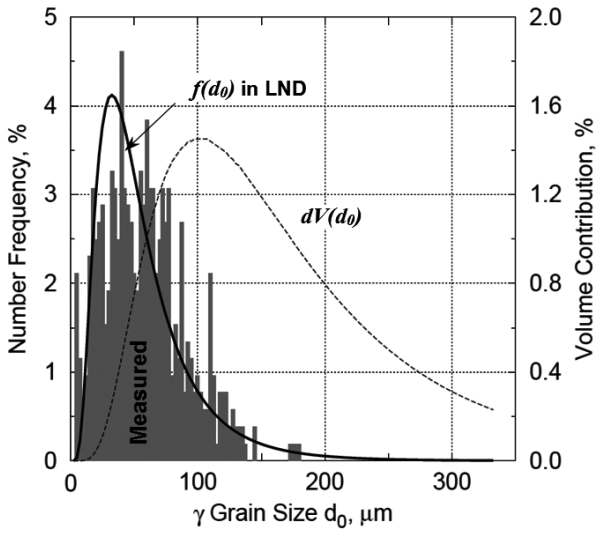

Fig. 2 Number frequency of γ grain size $f(d_0)$ in S steel austenitized at 1373 K for 70 s. The gray bars are the measured values, the solid line is the model in the log-normal distribution (LND), and the broken line is the volume contribution $d_V(d_0)$.

3. 3 Investigation of Kinetics and Final Microstructure

The specimens with and without hot working were continuously cooled below 673 K at rate of 10-120 K/min. Linear cooling was achieved by blowing a controlled Ar gas flow directly on the specimen. The sequential change of the α/*P*/*B* kinetics was validated by the interrupted microstructures following an He-gas quench during cooling. The microstructure was observed after chemical etching using a 2%-Nital solution. From the micrographs, the α, *P*, and *B* volume fractions were measured using a systematic point-counting procedure. A grid superimposed on the micrograph provided unbiased statistics regarding the particular phases of interest.

4. Results and Discussion

4. 1 Continuous Cooling Transformation Kinetics

Figures 3(a)-(c) show a series of quenched microstructures for the S steel, austenitized at 1373 K for 70 s and cooled at 40 K/min. In Fig. 3(a), for the sample quenched at 941 K, very thin α platelets (bright) are observed at the former positions of γ grain boundaries in the martensite matrix, and *P* nodules (dark) are visible adjacent to the α network in Fig. 3(b) for the sample quenched at 879 K. For the sample quenched at 851 K, shown in Fig. 3(c), a group of aligned plates can be seen in the remaining matrix, which is characteristic of the formation of α_B.

The α, *P*, and *B* fractions measured from these micrographs are compared with the calculated evolution curves in **Figs. 4**(a)-(c) for cooling rates of

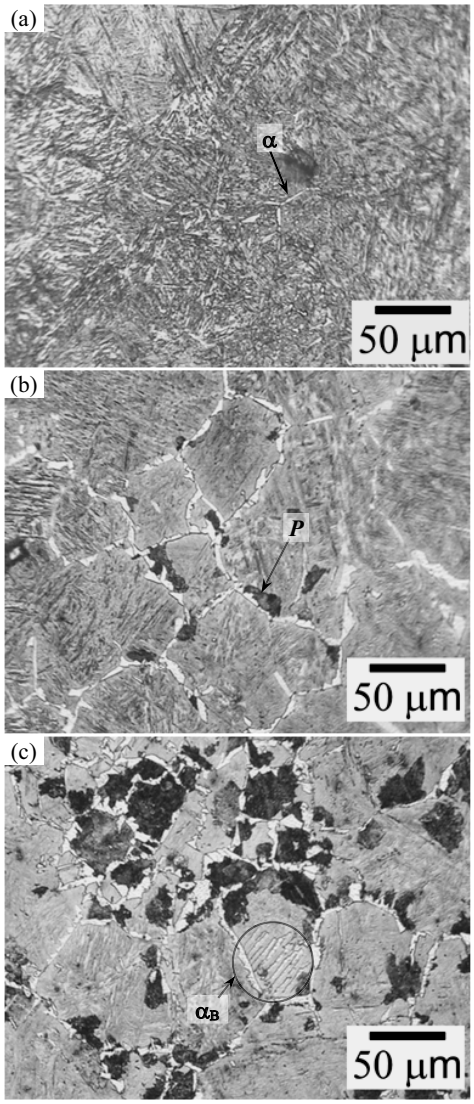

Fig. 3 Changes in quenched-out microstructures at (a) 941K, (b) 879K, (c) 851K during continous cooling of S steel at 40K/min.

10, 40, and 100 K/min, respectively. As the cooling rate increases, the α fraction (V_f) decreases and the transition to *P* occurs at lower temperatures. The calculated curves reproduce these α and *P* kinetics reasonably well. The *B* appears only for cases of faster cooling, as shown in Figs. 4(b) and (c). Although the experimental onset temperature cannot be clearly identified, it is approximately 823 K, whereas the calculation predicts 803 K. Despite this discrepancy, the energy criteria for α_B formation can be concluded to be applicable to *B* formation from γ_U following successive α-*P* transformations.

4. 2 Final Fractions After Cooling

Because of the simplicity of the present model, the dynamic evolution of *B* cannot be validated in detail. On the other hand, the final fractions of α, *P*, and *B* following cooling must be successfully predicted to avoid the intervention of *B* in real forgings. Particularly, the effect of the Mn content is of interest and is known to substantially influence the final microstructure. In **Figs. 5**(a)-(d), the final microstructures of samples cooled at 40 K/min and 100 K/min are compared to reveal the difference in the *B* fraction for the S and LM steels. Areas of aggregated fine α platelets are designated as *B*. Comparing cases for the same cooling rate, it is clear that the slightly higher Mn content in S steel promoted the *B* transformation in the α + *P* microstructure.

The α, *P*, and *B* fractions for different cooling rates are summarized in **Figs. 6**(a)-(c) for the three steels. The α and *P* fractions are added together for the stacked line plots, so that the remainder from unity gives the *B* fraction. In Figs. 6(a)-(c), the lowest

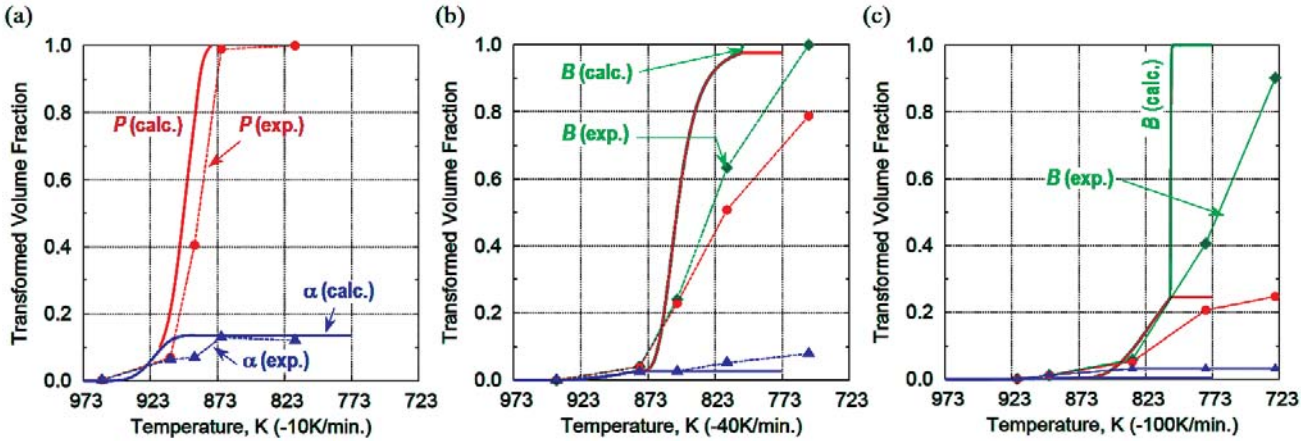

Fig. 4 Comparison of transformation kinetics of S steel during continuous cooling at (a) 10 K/min, (b) 40 K/min, and (c) 100 K/min.

cooling rate that gives rise to *B* formation is 30, 40, and 50 K/min, respectively, and thus increases with decreasing Mn content in the steels. The stacked bars represent the calculated results. Overall, the agreement between the experiments and calculations is reasonable for cooling rates of less than 70 K/min, and poor for cooling at 100 K/min. In view of the objectives of this modeling, the large differences among the three steels are well reproduced and the critical cooling rates for *B* formation agree with the experimental results quite nicely.

The final fractions were investigated also for the specimens cooled after hot compression. As shown in **Table 2**, the differences in hot deformation conditions, i.e., the initial γ diameter, deformation temperature affect the average recrystallized γ diameter, d_0. Recrystallization of γ grains finishes very quickly and the grains grow to sizes of up to about a hundred micrometers.

Figure 7 compares the experimental and calculated fractions. It can be seen that even for small changes in d_0, the calculation predicts the detailed changes in the α, *P*, and *B* fractions.

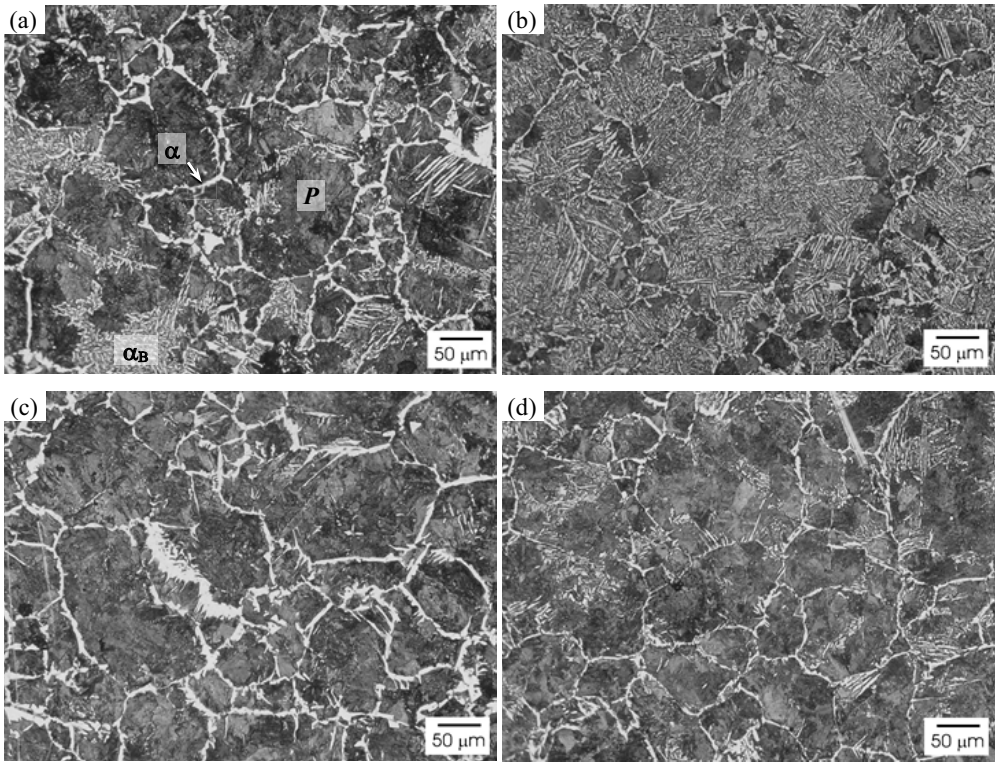

Fig. 5 Final microstructure of (a) HM, (c) S steel cooled at 40K/min, and (b)(d) S steel cooled at 100 K/min.

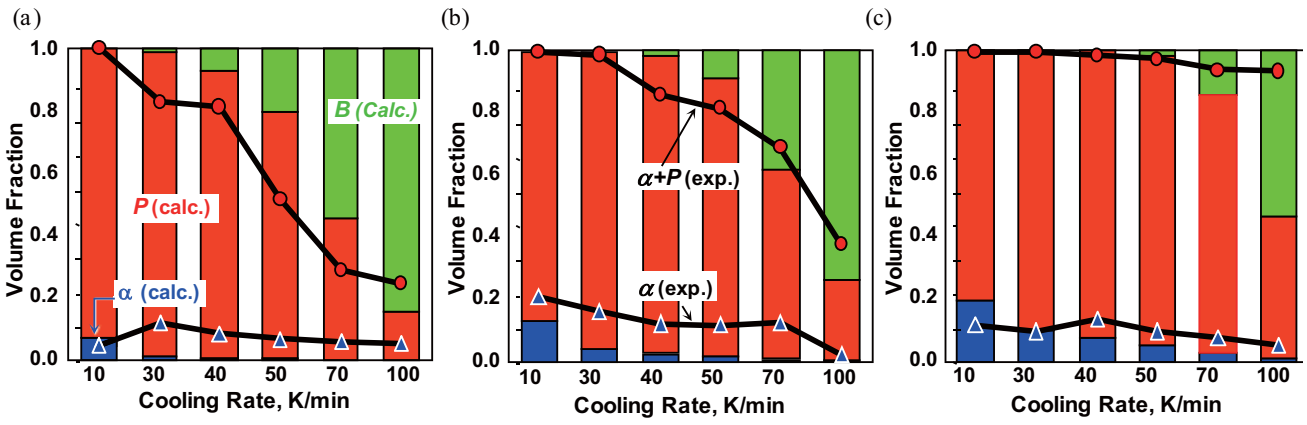

Fig. 6 Comparison of final volume fractions after continuous cooling, (a) HM, (b) S, and (c) LM steel.

Table 2 Hot deformation conditions for recrystallization, recrystallized γ diameter and cooling rate for phase transformation.

Specimen No	Initial γ diameter (μm)	Defomation condition Temperature(K)	Reduction	Holding time(s)	Recrystaled γ diameter(μm)	Cooling rate (K/min)
1	100	1273.15	50%	10	24	30
2	100	1273.15	50%	10	24	60
3	100	1473.15	50%	10	40	30
4	100	1473.15	50%	10	40	60
5	510	1473.15	50%	10	105	30
6	510	1473.15	50%	10	105	60

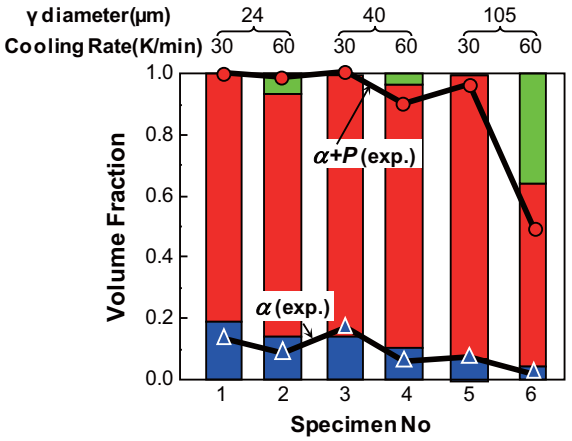

Fig. 7 Comparison of final volume fractions after continuous cooling for different γ grain diameters.

4. Conclusions

A model for successive α-*P*-*B* formation from γ_U has been proposed with particular emphasis on the continuous cooling of MCFS. New features of the model include a time-dependent growth rate and NPLE at the γ/α interface, which were used to provide a Mn-content-sensitive description of the preceding α transformation kinetics. This was enabled by the recursive evaluation of C enrichment in γ and a direct link to CALPHAD thermodynamic calculations. The energy criteria for α_B were first applied to the changing chemistry of γ_U during the α-*P* transformation. This method showed the ability to predict the formation of *B* due to minor variations in Mn content.

Acknowledgements

The authors acknowledge the financial support of the Japan Science and Technology Agency (JST). K. Tanaka would like to thank the members of the Phase Transformation Group in CENIM for fruitful discussions.

References

(1) Bhadeshia, H. K. D. H., *Acta Metall.*, Vol.29 (1981), pp.1117-1130.
(2) Rees, G. I. and Bhadeshia, H. K. D. H., *Mater. Sci. Technol.*, Vol.8 (1992), pp.985-993.
(3) Chester, N. A. and Bhadeshia, H. K. D. H., *J. Phys. IV France*, Vol.7 (1997), C5-41-46.
(4) Azuma, M., Fujita, N., Takahashi, M., Senuma, T., Quidort, D. and Lung, T., *ISIJ International*, Vol.45 (2005), pp.221-228.
(5) Santofimia, M. J., Caballero, F. G., Capdevila, C., García-Mateo, C. and García de Andrés, C., *Mater. Trans.*, Vol.47 (2006), pp.2473-2479.
(6) Santofimia, M. J., Caballero, F. G., Capdevila, C., García-Mateo, C. and García de Andrés, C., *Mater. Trans.*, Vol.47 (2006), pp.2465-2472.
(7) Garcia-Mateo, C. and Bhadeshia, H. K. D. H., *Mater. Sci. Eng.: A*, Vol.378 (2004), pp.289-292.
(8) Umemoto, M., *Proc. Int. Symp. on Mathematical Modeling of Hot Rolling of Steel* (1990), pp.404-423.
(9) Suehiro, M., Senuma, T., Yada, H., Matsumura, Y. and Ariyoshi, T., *Tetsu-to-Hagane* (in Japanese), Vol.73 (1987), pp.1026-1033.
(10) Jones, S. J. and Bhadeshia, H. K. D. H., *Acta Mater.*, Vol.45 (1997), pp.2911-2920.
(11) Parker, S. V., Ph.D. Thesis (1997), University of Cambridge.
(12) Senuma, T., Yada, H., Matsumura, Y. and Nimura, T., *Tetsu-to-Hagane* (in Japanese), Vol.70 (1984), pp.2112-2119.
(13) Lange, W. F., Enomoto, M. and Aaronson, H. I., *Metall. Trans. A*, Vol.19 (1988), pp.427-440.
(14) Capdevila, C., Andrés, C. G. and Caballero, F. G., *Scripta Mater.*, Vol.44 (2001), pp.129-134.
(15) Bhadeshia, H. K. D. H., David, S. A., Vitek, J. M. and Reed, W., *Mater. Sci. Technol.*, Vol.7 (1991), pp.686-689.
(16) Liu, X., Kayjalainen, P. and Perttula, J. S., *Proc. 2nd*

Int. Conf. on Modeling of Metal Rolling Processes (1996), pp.489-500.
(17) Capdevila, C., private communication.
(18) Sietsma, J. and van der Zwaag, S., *Acta Mater.*, Vol.52 (2004), pp.4143-4152.
(19) Hutchinson, C. R., Fuchsmann, A. and Bréchet, Y., *Metall. Mater. Trans. A*, Vol.37 (2006), pp.1711-1720.
(20) Hutchinson, C. R., Zurob, H. S. and Bréchet, Y., *Metall. Mater. Trans. A*, Vol.35 (2004), pp.1211-1221.
(21) Tanaka, K., Hara, M., Yogo, Y., Nakanishi, K. and Capdevila, C., *CAMP-ISIJ: Proc. 155th ISIJ Meeting*, Vol.21 (2008), pp.469-470.
(22) Capdevila, C., Caballero, F. G. and Andrés, C. G., *Acta Mater.*, Vol.50 (2002), pp.4629-4641.
(23) Aaronson, H. I., Plichta, M. R., Franti, G. W. and Russell, K. C., *Metall. Trans. A*, Vol.9 (1978), pp.363-378.
(24) Reed, R. C. and Bhadeshia, H. K. D. H., *Mater. Sci. Technol.*, Vol.8 (1992), pp.421-435.
(25) Hillert, M. and Höglund, L., *Scripta Mater.*, Vol.50 (2004), pp.171-173.
(26) Capdevila, C., Caballero, F. G. and Andrés, C. G., Vol.50 (2004), pp.175-177.
(27) Takahashi, M., Ph.D. Thesis (1992), University of Cambridge.

Fig. 1
Reprinted from Materials Transactions, Vol.50, No.3 (2009), pp.551-555, Tanaka, K., Yogo, Y., Nakanishi, K. and Capdevila, C., Prediction of Bainite Intervened in Ferrite-Pearlite Forging Steel, I. Modeling, © 2009 The Japan Institute of Metals, with permission from the Japan Institute of Metals.

Figs. 2-6 and Table 1
Reprinted from Materials Transactions, Vol.50, No.3 (2009), pp.556-561, Tanaka, K., Hara, M., Nakanishi, K. and Capdevila, C., Prediction of Bainite Intervened in Ferrite-Pearlite Forging Steel, II. Experimental Evaluation, © 2009 The Japan Institute of Metals, with permission from the Japan Institute of Metals.

Hideaki Ikehata
Research Fields:
- Physical Metallurgy
- Steels
- Metals and Alloys

Academic Societies:
- The Iron and Steel Institute of Japan
- The Japan Society for Heat Treatment
- The Japan Institute of Metals

Kouji Tanaka
Research Fields:
- Physical Metallurgy
- Steels
- Metals and Alloys

Academic Degree: Dr.Eng.
Academic Societies:
- The Iron and Steel Institute of Japan
- The Japan Society for Heat Treatment
- The Minerals, Metals and Materials Society

Awards:
- The Japan Institute of Metals Technical Development Award, 1996
- R&D100 Award, 1998
- 11th GTSJ Dissertation Award, 2002

Carlos Capdevila*
Research Fields:
- Physical Metallurgy
- Steels
- Metals and Alloys

Academic Degree: Dr.Sci.
Academic Societies:
- The Minerals, Metals and Materials Society
- Sociedad Española de Materiales (SOCIEMAT)
- European Materials Research Society (E-MRS)

Award:
- Vanadium Award, 2008

*Centro Nacional de Investigaciones Metalurgicas (CENIM-CSIC)

